ADVANCED FUNCTIONAL MATERIALS
www.afm-journal.de

Removal of Steroid Hormone Micropollutants by an Electrochemical Carbon Nanotube Membrane Flow-Through Reactor: Role of Concentration and Degradation Mechanisms

*Siqi Liu, David Jassby, and Andrea I. Schäfer**

The sustainable provision of water is a major global challenge, exacerbated by increasing micropollutant contamination. Developing advanced treatment processes and understanding the fundamental mechanisms responsible for the water purification processes are therefore imperative. The removal of steroid hormone (SH) micropollutants at environmentally realistic concentrations is investigated using a flow-through electrochemical membrane reactor (EMR) equipped with a carbon nanotube membrane. This EMR is a novel micro design, minimizes typical mass transfer limitations across varying system parameters, and enables an in-depth study of the limiting factors at extremely low SH concentrations, typical for micropollutants. The integration of high-performance liquid chromatography with a flow scintillator analyzer and liquid scintillation counting techniques allows elucidation of the complex interplay between adsorption, degradation, and byproduct transformation that takes place in the EMR. A permeate concentration below the detection limit (<2.5 ng L^{-1}) is achieved in the reactor, with the heterogeneous electron transfer identified as the main pathway for steroid hormones degradation. The apparent rate of SH removal in the EMR is linear in the concentration range of 50 to 5×10^4 ng L^{-1}. These findings indicate good potential of EMR for SH removal and provide new knowledge for designing and optimizing the EMR process.

1. Introduction

Water contamination by micropollutants represents a pressing global issue, and steroid hormones (SHs) pose a particular risk.[1–4] These substances, which include both naturally occurring and synthetic hormones such as estrone (E1), 17β-estradiol (E2), progesterone (P), and testosterone (T) are frequently detected in various water bodies.[5–7] SHs are potent endocrine disruptors, posing a significant risk to human and environmental health.[8–11] Even at concentrations as low as ng L^{-1}, these substances can cause extensive developmental and reproductive adverse effects in both humans and wildlife and can destabilize aquatic ecosystems.[12,13] In response to these threats, stringent regulatory guidelines for SHs in water have been established. The European Union (EU), for example, has set an annual average environmental quality standard of 0.4 ng L^{-1} for E2 in surface water.[14] This highlights the urgent necessity for effective treatment of these micropollutants at relevant concentrations, where mass transfer is a major limitation.

The most commonly used processes in municipal wastewater treatment plants often fall short in efficiently removing SHs.[15–17] While nanofiltration (NF) membranes have demonstrated SH micropollutant retention of 10–100%,[18–20] their practical implementation faces two critical limitations: i) the production of concentrated waste streams requiring costly secondary treatment,[21,22] and ii) energy-intensive operation under high pressures (≈5–20 bar). For instance, Imbrogno et al.[23] achieved ≈75% E2 removal from a 100 ng L^{-1} solution using NF90 and NF270 membranes, but this required pressures of 9.6 bar with modest fluxes (77–135 L m^{-2} h^{-1}). Integrating membrane processes with photocatalysis has achieved SH removal exceeding 80% at higher flux (150 L m^{-2} h^{-1}) and far lower pressure (≈0.03 bar) in laboratory studies.[24–26] However, the effectiveness of photocatalysis relies on light penetration within the system,[27] lacking process upscaling and continuous application in real water.

S. Liu, A. I. Schäfer
Institute for Advanced Membrane Technology (IAMT)
Karlsruhe Institute of Technology (KIT)
Hermann-von-Helmholtz-Platz 1, 76344 Eggenstein-Leopoldshafen, Germany
E-mail: andrea.Iris.schaefer@kit.edu
D. Jassby
Department of Civil and Environmental Engineering
University of California, Los Angeles
Los Angeles, CA 90095, USA

The ORCID identification number(s) for the author(s) of this article can be found under https://doi.org/10.1002/adfm.202510813

DOI: 10.1002/adfm.202510813

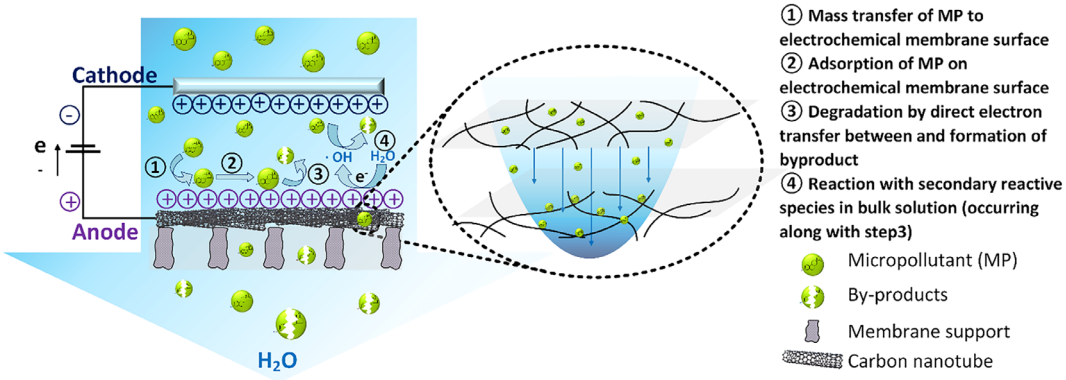

Figure 1. Schematic of the electrochemical membrane reactor using a carbon nanotube (CNT) membrane anode and a titanium cathode for neutral steroid hormone micropollutants with a high affinity for CNT in dead-end filtration.

Electrochemical oxidation can overcome some of these constraints by applying a uniform potential over the electrode surface, thereby offering highly efficient degradation of a broad range of recalcitrant micropollutants.[28–30] In this process, the fine-tuning of electrochemical potential results in alterations in i) electron concentration and ii) electron energy levels at the electrode interface. The process aims to exploit electrons adsorbed at the electrodes by Faradaic electron transfer to drive direct chemical transformations.[31,32] The chemical reaction involves the loss of electrons by a molecule at the anode, leading to its oxidation, while electrochemical reduction—the counterpart to electrochemical oxidation—occurs through the gain of electrons by a molecule at the cathode. Ngundi et al.[33] investigated the electrochemical behavior of E2 at a platinum electrode, noting oxidation at 1 V versus Ag/AgCl and the formation of a quinone product.

In addition to direct degradation mechanisms, the interaction of water or other species at the electrode surface leads to the in situ generation of various reactive species that tend to govern the indirect degradation of micropollutants in many electrochemical systems.[34,35] Notably, the hydroxyl radical (·OH), produced as an intermediate in the oxidation of water or by reactions involving H_2O_2 on specific catalysts, such as in a Fenton-like reaction.[36] It is believed to be one of the most important species in these oxidative processes,[37] even though the identification of reaction pathways and kinetics is far from understood. A distinct category of oxidizing agents is formed from the oxidation of chloride ions to generate active chlorine, which effectively oxidizes a wide range of contaminants[38,39] but can result in the formation of organochlorinated disinfection byproducts.[40]

Despite the appealing features of electrochemical technologies, the mass transport of micropollutants from the bulk solution to the electrode surface limits the reaction rates and hinders the broader application of this technology.[41,42] Electrochemical membrane reactors (EMRs) effectively address the mass transport challenge by integrating membrane filtration with electrochemically driven reactions.[43–47] Electrochemical membranes (EMs), the core component of the EMR, function as porous flow-through electrodes with nm-sized pores, with an electrochemical potential applied against a counter electrode (**Figure 1**). The EMs operate by synergistically combining membrane separation and electrochemical reactions, spatially confined within the nano-scale intraporous structures of the membrane.[48] The spatial confinement within the pore channels of the EMs, ranging from a few tens of nm to <1 µm, results in a compressed diffusion layer that enriches the concentration of micropollutants near the reactive sites on the membrane surface.[41,49] This configuration enhances the contact between micropollutants and active sites. In turn, both adsorption and reaction kinetics are improved, resulting in a more efficient contaminant degradation rate. A previous study[41] it was suggested that the contribution of direct electron transfer versus indirect degradation is influenced by the membrane pore size in the EMR. Smaller pores compress the diffusion layer and lead to an increased local reactant concentration near the electrode surfaces. This enhances the likelihood of direct interactions between the membrane and micropollutant that enable direct electron transfer. Naturally, fluid dynamics within the porous structure, particularly the convective flow and diffusion, play a crucial role in enhancing contact between micropollutants, reactive species, and electrode surfaces.[43,50] This requires careful identification of the limiting factors at realistic concentrations.

Carbon nanotubes (CNTs) are the most common material for the fabrication of EM due to their unique physicochemical properties,[51] such as high conductivity (1000–200 000 S cm^{-1} for multi-walled CNTs),[52–54] large surface areas (50–1000 m^2 g^{-1}),[55] strong affinity for a wide range of organic compounds,[56] exceptional mechanical strength,[57] and large aspect ratios.[52] Liu et al.[58] investigated the treatment of aqueous antibiotics, tetracycline (TC), using a CNT electrochemical filter. The results showed an oxidative flux of 0.0025 ± 0.001 mol m^{-2} h^{-1} at cell voltage of 2.5 V, flow rate (1.5 mL min^{-1}, hydraulic residence time, HRT < 2 s), and initial TC concentration of 0.2 mM. Dos Santos Cunha et al.[59] investigated the performance of an electrochemical CNT membrane (with a pore size of 15 nm) as anode in the oxidation of E2 (10 mg L^{-1}) and 17α-ethinylestradiol (EE2, 11 mg L^{-1}). The highly concentrated SH was both dissolved in acetonitrile. Removal of >99% for these compounds via adsorption and degradation was reported, although the contributions of each process could not be differentiated. CNT EMs exhibit promising oxidation capabilities, but long-term performance tends to decline due to the compromised stability of CNTs under sustained anodic potentials.

While research to date has indicated feasibility and provided valuable insights into membrane electrocatalysis treatment targeting micropollutants, the majority of these studies utilized synthetic solutions at unrealistically high concentrations. This results in significant challenges when findings are to be translated to environmentally realistic scenarios where concentrations of micropollutants are substantially lower and other water contaminants interfere with electrode reactions. Prior studies have shown that electrooxidation experiments with high initial micropollutant concentrations tend to overestimate the performance of the process due to an increased diffusion flux caused by a larger concentration gradient.[61] Such an overestimation hampers application to the treatment of most contaminated waters, no matter if ground-, surface- or waste- waters, where micropollutant concentrations are low. Investigating micropollutant removal at realistic concentrations is challenging as the detection limits are near the guideline values. Nevertheless, realistic concentrations are critical as this provides in-depth insight into reaction kinetics and mechanisms, which often differ from those observed at higher concentrations.

In this study, the removal of SH micropollutant and the responsible mechanisms using a CNT EMR at an environmentally relevant SH concentration (100 ng L^{-1}) was examined. This required an integrated analytical approach using ultra-high-performance liquid chromatography-flow scintillator analyzer (UHPLC-FSA) coupled with liquid scintillation counting (LSC) technique that enables differentiation of simultaneous adsorption, desorption, and degradation processes. The methodology was previously developed and validated[61] using a larger-scale model (20 cm^2) to ensure sufficient adsorption capacity, which was critical for establishing baseline parameters and demonstrating the applicability across diverse systems and materials. In this work, a downscaled EMR, reducing the EM area from 20 to 2 cm^2, was established to overcome a fundamental limitation of the large-scaled system: excessive adsorption capacity obscures degradation kinetics. At realistic concentrations (100 ng L^{-1}), the high surface area of larger models creates dominant adsorption sites relative to trace pollutant levels, rendering other removal mechanisms negligible and mechanistically unobservable. The downscaled configuration facilitates a more in-depth investigation of primary limiting factors affecting micropollutant removal at lower concentrations. Here, the main objective being i) to investigate the predominant mechanisms, such as adsorption, direct electrons transfer and/or secondary reactive species, for SH degradation in the CNT EMR, ii) to determine the limiting factors for the electrochemical adsorption and degradation of SH, as well as byproduct formation, and iii) to gain deeper understanding in the influence of concentration on degradation behavior of SH micropollutant, all in synthetic water.

2. Results and Discussion

The SH removal of the EMR was evaluated at a concentration of 100 ng L^{-1}, elucidating the specific degradation mechanism (direct electron transfer vs indirect reactive species), and gaining a better understanding of the limiting factors by distinguishing the concurrent electrochemical adsorption and degradation.

2.1. Estradiol Removal Achieved with Electrochemical Membrane

To quantify estradiol (E2) at an environmentally realistic concentration of 100 ng L^{-1} removal by adsorption or degradation within the downscaled CNT EMR system was investigated. A volume of 200 mL to attain saturation without voltage and a further 500 mL for electrocatalysis at a cell voltage 1.6 V was operated at a flux 600 L m^{-2} h^{-1} (**Figure 2**).

In the absence of the externally applied voltage, a consistent increase in the normalized E2 concentration in permeate (c_p/c_f) was observed, rising from 0.03 ± 0.02 to 0.72 ± 0.1 over a permeate volume of 200 mL (Figure 2A), indicating that saturation was not achieved (value of 1). Upon applying a cell voltage of 1.6 V across the electrode pairs, the normalized E2 concentration decreased dramatically, ultimately stabilizing at 0.02 ± 0.01, which corresponds to a removal of >97.5% as the LOD of the analytical tool is 2.5 ng L^{-1} (see Figure S7, Supporting Information). This high removal was achieved at a notably high flux (600 L m^{-2} h^{-1}) and relatively low operating pressure (2.5 bar), highlighting the operational advantages of CNT EMR over alternative technologies, such as NF and photocatalytic membrane reactor (PMR). At 4–8 times higher flux and 3.8 times lower operating pressure, the CNT EMR simultaneously exceeded 75% E2 removal of NF90 and NF270.[23] Though PMRs using different membranes (PES-TiO_2[26] and PVDF-TiO_2[27]) reached comparable removal (94–96%), the CNT EMR drastically reduced external energy consumption (6.7×10^{-5} kWh) through a low-voltage (1.6 V) electrochemical degradation mechanism, avoiding the substantial energy requirements of light irradiation (≈3.5×10^{-3} kWh). Note that these energy estimates represent laboratory-scale approximations which exclude real-world efficiency losses and systemic power conversion factors. The detailed comparisons are provided in Table S8 (Supporting Information).

Concurrent with the decrease in E2 concentration, three distinct degradation products were identified by their characteristic retention times at ≈3, 5, and 8 min using UHPLC-FSA (Figure 2D). The normalized concentration of byproduct-3m surged to 0.72 ± 0.08 immediately after activating the voltage, then decreased and plateaued at ≈0.35 ± 0.04 with further filtration (Figure 2B). The normalized concentrations of byproduct-5m and -8m were consistently lower than that of byproduct-3m, reaching 0.15 ± 0.03 by the end of the experiment (Figure 2B).

The normalized ^3H concentration, reflecting the total amount of radiolabeled E2 and its degradation products present in the permeate, was observed to rise beyond 1 after the cell voltage was applied (Figure 2C). This increase indicated the desorption of either E2, its degradation products, or a combination of both from the membrane surface. Moreover, the normalized ^3H activity in the permeate was determined to be commensurate with the aggregate concentrations of intact E2 and its three transformation products. This finding suggested that these three byproducts are the principal byproducts of E2 degradation in the CNT EMR.

The removal performance of this micro-CNT EMR system (2 cm^2) was comparable to that of a previously used larger-scale model (20 cm^2),[61] which achieved 92 ± 4% E2 removal by the end of the experiment. The same byproducts were observed at 3, 5, and 8 min, even though an initial concentration that was 10 times higher (1000 ng L^{-1}) was used. Previous work[61] suggested that unrealistically high micropollutant concentrations (usually

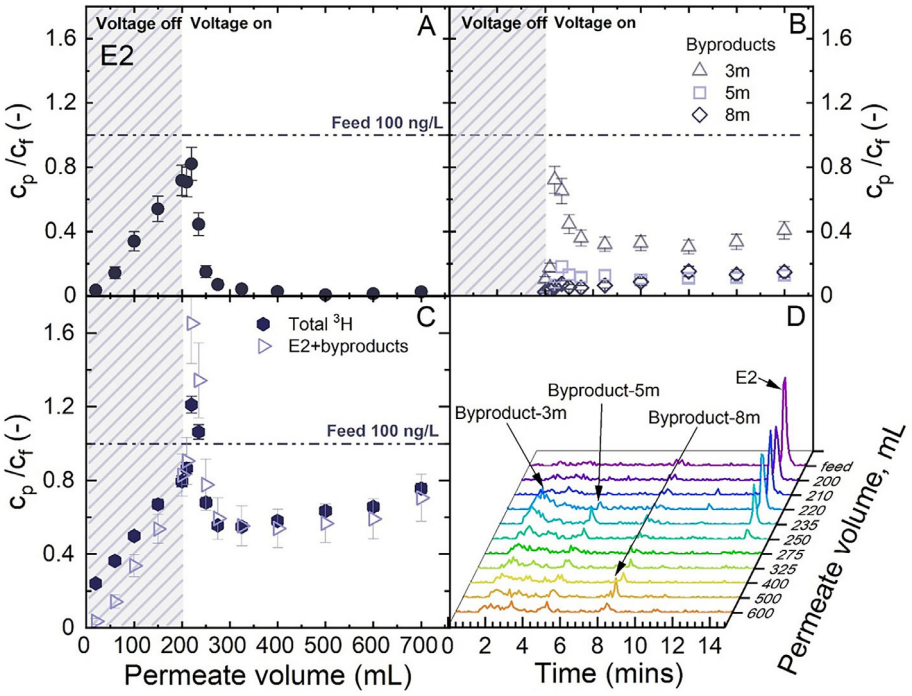

Figure 2. Normalized concentration of A) E2 ($c_{p,E2}/c_{f,E2}$), B) byproducts ($c_{p,met}/c_{f,met}$), C) ^{3}H, and the sum of E2 and the three byproducts versus accumulated permeate volume, and D) UHPLC-FSA chromatograms of E2 during the electrochemical degradation with increasing accumulated permeate volume. $c_{f,E2}$ = 100 ng L^{-1}, V_{cell} = 1.6 V, J_f = 600 L m^{-2} h^{-1} (2 mL min^{-1}), 1 mM $NaHCO_3$, 10 mM NaCl, 27.2 mg L^{-1} EtOH, 79.2 mg L^{-1} MeOH, pH 8.2 ± 0.2, 23 ± 0.2 °C. Error bars represent propagated error from operational parameter variations and analytical error.

several orders of magnitude higher) in batch mode likely overestimate the electrooxidation performance due to the enhanced concentration gradient. This micro-CNT EMR allowed for the investigation of SH removal and its underlying mechanisms at environmentally realistic concentrations (100 ng L^{-1}), a condition not feasible in the large model, where reaction kinetics were consistently limited by SH availability.

2.2. Degradation Dependence on Micropollutant Concentration

To verify the removal dependence on the initial micropollutant concentration within a flow-through EMR, the electrochemical filtration experiments were performed across a broad concentration range, varying from 50 to 10^6 ng L^{-1} (**Figure 3**). The progression of the normalized permeate concentration of E2, ^{3}H activity, and the formed byproducts (−3m, 5m, 8m) over permeate volume, as well as the UHPLC-FSA chromatograph over the cumulative permeate volume for all electrochemical filtration experiments are detailed in Figures S16–S26 (Supporting Information). System parameters, such as conductivity, pH, temperature, and transmembrane pressure recorded during the experiments can be found in Figures S18,S21,S22,S27 (Supporting Information).

Figure 3A shows a strong linear correlation for the apparent rate of E2 removal as a function of its initial concentration, ranging from 50 to 5 × 10^4 ng L^{-1}, before levelling out at concentrations above 5 × 10^4 ng L^{-1}. This pattern indicated a reaction regime constrained by the availability of E2 molecules at the membrane surface below 5 × 10^4 ng L^{-1}. Notably, the apparent removal rate reached a maximum of (3.8 ± 2.9) × 10^{-9} mol m^{-2} s^{-1} when E2 concentration surpassed 5 × 10^4 ng L^{-1}. This sharp shift marked the transition from a concentration-limited regime to one governed by surface area, where the reactive sites on the membrane interface are saturated with E2. The strong linear correlation depicted in Figure 3A indicated that the apparent removal rates observed at higher concentrations can be extrapolated to lower concentrations within the concentration-limited region in this case. This can be attributed to the significantly enhanced mass transfer within the EMR, where diffusion becomes negligible due to the convective flow and possibly the high adsorption by the CNT.

Elevated pollutant concentrations typically lead to increased production of byproducts. If these are adsorbed on the membrane and the surface area is limited, the interaction between E2 with the active sites can be hindered and thus slow down degradation. Here, the formation rates of all three byproducts increased linearly with E2 concentration ranging from 50 to 5 × 10^4 ng L^{-1} (Figure 3B), indicating that the surface is probably not limited. The balance of ^{3}H concentration in the permeate with the cumulative concentration of E2 and its byproducts indicates the absence of other byproduct types (Figure 3C). This outcome is likely due to the fact that the internal surface area is large and/or a high desorption of byproducts, which prevents passivation of the membrane electrode.

At concentrations exceeding 5 × 10^4 ng L^{-1} under the examined conditions (1.6 V and a flux of 600 L m^{-2} h^{-1}), the concentration-limited regime is exceeded and extrapolating the removal rate across different concentrations is no longer

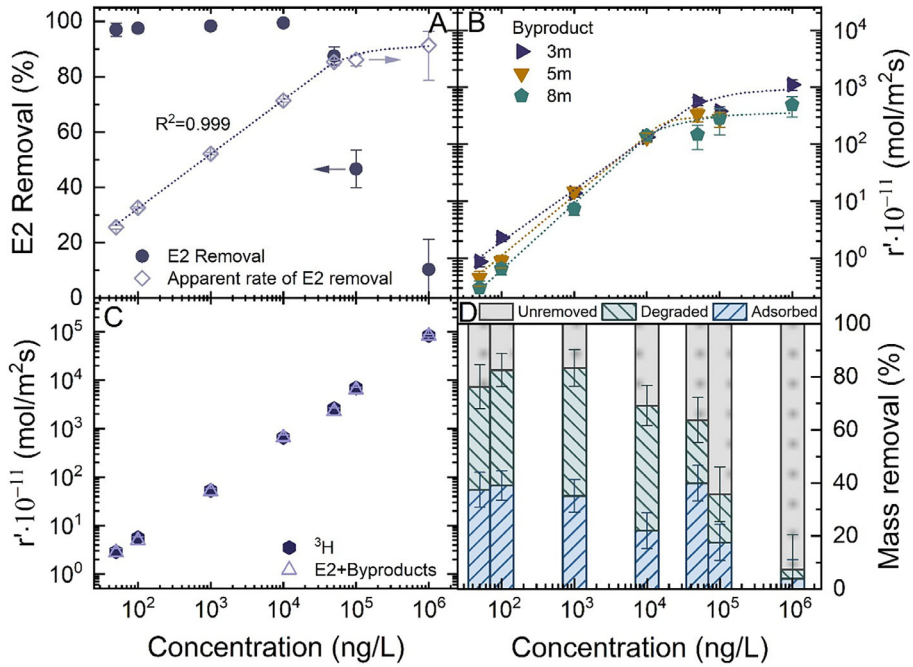

Figure 3. Electrochemical degradation of estradiol (E2) over concentration from 50 to 10^6 ng L^{-1}, expressed as A) E2 removal and apparent rate of E2 removal, B) apparent rate of byproduct formation, C) ^3H, and the sum of E2 and the three byproducts in permeate; and D) contribution to the mass removal of E2 by the electrochemical adsorption and degradation versus concentration. $c_{f,E2}$ = 100 ng L^{-1}, V_{cell} = 1.6 V, J_f = 600 L m^{-2} h^{-1} (2 mL min^{-1}), 1 mM $NaHCO_3$, 10 mM NaCl, 27.2 mg L^{-1} EtOH, 79.2 mg L^{-1} MeOH, pH 8.2 ± 0.2. 23 ± 0.2 °C. Error bars represent propagated error from operational parameter variations and analytical error.

possible. This highlights that identifying the limiting factors of the EMR under varying operational parameters is critical. Before delving into these limiting factors, the primary degradation mechanisms (i.e., direct electron transfer vs indirect transfer via reactive species) will be elucidated.

2.3. Mechanism of Estradiol Degradation with the Electrochemical Membrane

To understand the degradation mechanisms (direct vs indirect) within the CNT EMR, key reactive species, notably •OH,[49,62] and reactive chlorine (Equations (S1)–(S5),[63,64] Supporting Information), were initially identified across a range of cell voltages (from 0.9 to 3 V).

2.3.1. Indirect Oxidation by Reactive Species

As shown in Figure S9 (Supporting Information), within the examined voltage range, neither active chlorine nor •OH was detected, indicating their negligible contribution to E2 degradation. This observation aligns with previous studies, which suggest that indirect oxidation at CNT electrodes is likely minimal at low voltages.[65,66] It is important to note that the lack of •OH detection could be due to either; i) negligible •OH production on the CNT membrane under the given voltage conditions, or ii) the presence of high concentrations of scavengers such as EtOH (0.57 mM), MeOH (2.5 mM), and HCO_3^- (1 mM) in the water matrix, all of which are strong •OH scavengers.[67] In either case, •OH would not have contributed to the degradation of E2 under these conditions.

2.3.2. Oxidation by Direct Electron Transfer

These findings lead to the assumption that direct electron transfer is the predominant mechanism for SH degradation, as evidenced by the fundamental electrochemical studies of SH on the CNTs membrane (**Figure** 4A), which were conducted using CV measurement in a plate cell (Figure S3, Supporting Information). To achieve an enhanced response signal, a high SH concentration of 1 mg L^{-1} was required.

As a control experiment, the CV measurement was conducted in the matrix solution, where no peaks were observed in either the oxidation or reduction scans. An anodic oxidation peak for E2 was observed at a potential of +0.75 V (vs Ag/AgCl,) while no corresponding reduction peak was detected in the reverse scan (Figure 4A). This was attributed to the irreversible electrooxidation of E2 via direct electron transfer on the CNTs membrane within the examined potential. This finding is in agreement with a prior study reporting electrooxidation of E2 (37 µM) with a CNT electrode at a similar potential of +0.76 V (vs Ag/AgCl).[59] The observed gradual decrease in the magnitude of the oxidative peak across successive scanning cycles implied a diffusion-controlled mechanism, where the rate of electron transfer appears significantly faster than the transport rates of E2 onto the CNTs surface in the plate cell.[68] It is worth noting that this decreasing peak

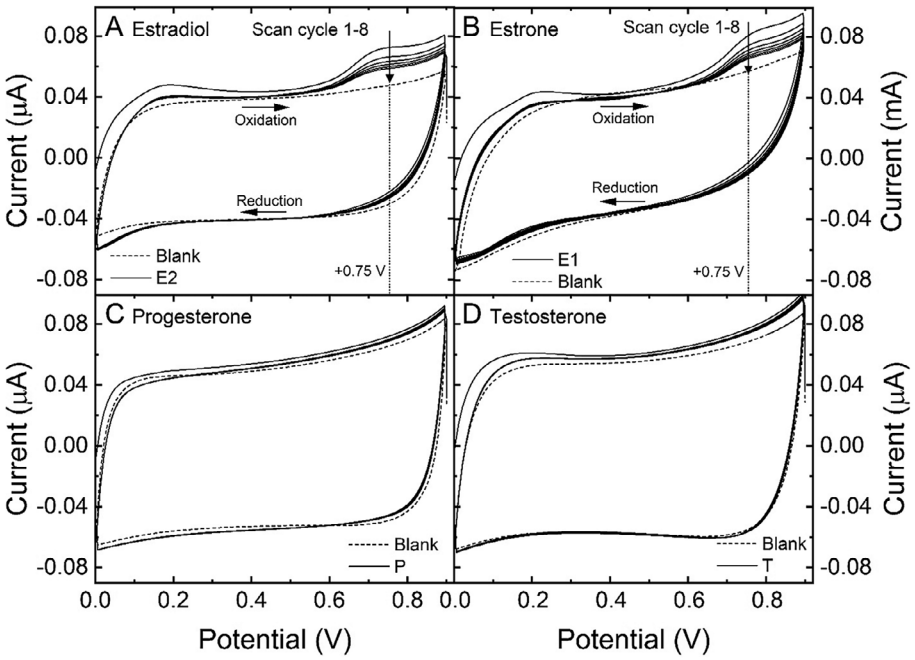

Figure 4. Cyclic voltammograms for 1 mg L^{-1} A) estradiol, B) estrone, C) progesterone, and D) testosterone in electrolyte containing 10 mM NaCl, 1 mM $NaHCO_3$, 27.2 mg L^{-1} EtOH, and 79.2 mg L^{-1} MeOH in potentential range from 0 to 0.9 V with a scan rate of 100 mV s^{-1}.

may not be relevant to the EMR due to the improved mass transfer facilitated by the flow-through configuration and the high adsorption to the CNT membrane. In the EMR, the removal rate was limited by the concentration of E2 rather than mass transfer when below 5×10^4 ng L^{-1} (Figure 3).

To confirm the hypothesis of the dominance of the electron transfer mechanism in the E2 degradation, $NaNO_3$ was employed as a scavenger to target surface electrons (Figure S28, Supporting Information). The result showed that $NaNO_3$ significantly impeded the removal of E2 in the CNT EMR, with negligible formation of the degradation products during treatment. This confirmed that direct electron transfer predominates the degradation mechanism of E2 in the CNT EMR. These findings agreed well with those reported in previous studies[48] which noted that the sp^2 carbon-based electrodes typically serve as active anodes with an overpotential for O_2 evolution generally lower than 0.4 V (vs SHE).[69] The well-recognized model of anodic oxidation, initially proposed by Comninellis[65] and slightly modified by Marselli et al.,[66] suggested that these active anodes (M) form strong interactions with electrogenerated •OH to produce a higher state oxide (MO), $M(\cdot OH) \rightarrow MO + H^+ + e^-$. This oxide, in combination with the anode surface (redox couple MO/M), acts as a selective mediator in the degradation of organic compounds through direct electron transfer.

Having identified direct electron transfer as the primary mechanism enables a more detailed discussion of the degradation pathway of E2 in the CNT EMR, as outlined in the following section.

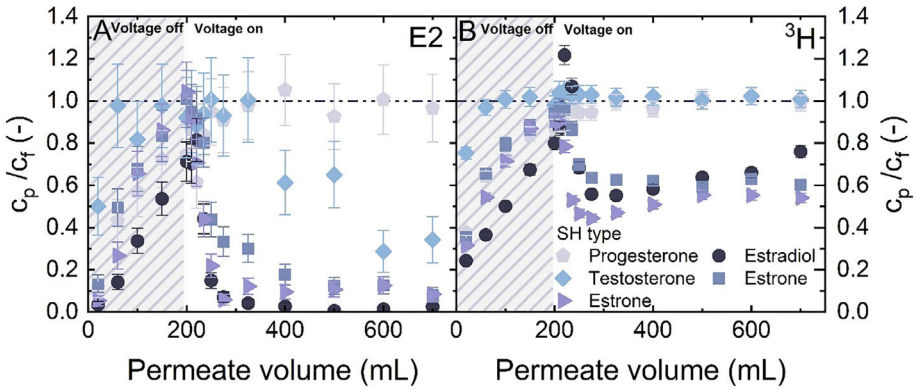

Figure 5. Normalized concentration of A) SH, and B) ^3H, versus permeate volume. $c_{f,SH}$ = 100 ng L^{-1}, V_{cell} = 1.6 V, J_f = 600 L m^{-2} h^{-1} (2 mL min^{-1}), 1 mM $NaHCO_3$, 10 mM NaCl, 27.2 mg L^{-1} EtOH, 79.2 mg L^{-1} MeOH, pH 8.2 ± 0.2, 23 ± 0.2 °C. Error bars represent propagated error from operational parameter variations and analytical error.

2.4. Products of Degradation of Estradiol via Direct Electron Transfer

Direct electron transfer is believed to involve E2 in the release of two protons (one in the phenol group and one at C9, Equation (1)) and the generation of a phenoxy radical. This phenoxy radical can then resonate within the aromatic ring, forming a ketone derivative.[33,70,71] Such a transformation is likely to diminish the estrogenic activity of E2, owing to significant chemical alteration of its phenolic binding group.[72,73] However, accurate identification of byproducts cannot be confirmed with the current analytical tools. It is important to investigate the estrogenic activity or toxicity of the treated SH solution in future studies and in real water, where additional byproducts and by-products may be generated.

Results showed that E1 and E2 were removed more efficiently than, T and P. No discernible removal of P was observed, whereas T exhibited a removal of 66 ± 11% at the end of the experiment. This indicated a considerably reduced electro-oxidative activity for T and P compared to E1 and E2, which is further supported by their voltametric analysis on the CNTs membrane (Figure 4). Distinct oxidation peaks were observed for E1 and E2 at +0.75 V (vs Ag/AgCl), while no notable peaks appeared for either T or P. Arvand et al.[74] observed oxidative peaks for E2 and P at +0.55 and +0.85 V (vs Ag/AgCl) respectively, using a modified graphene quantum dot electrode, which also suggested that E2 is more readily oxidized than P, attributing to the presence of a hydroxyl group in its aromatic ring.[75] The phenolic structure of E2 is enriched with delocalized π electrons, facilitating electron transfer processes through resonance in the aromatic structure.[76,77] E1,

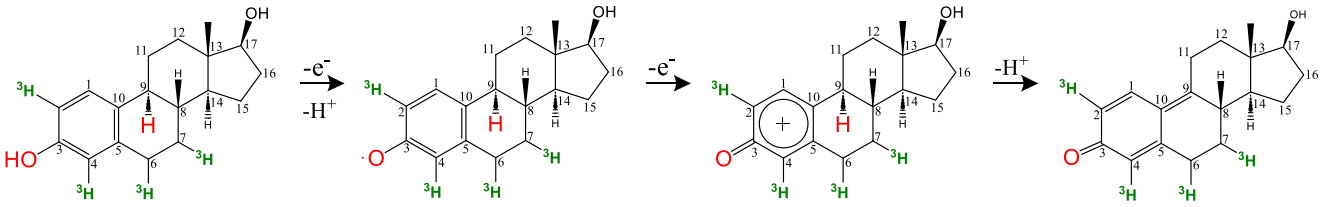

(1)

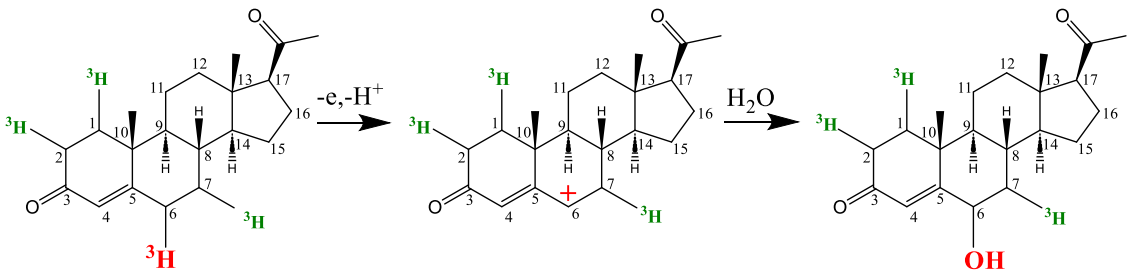

(2)

with a similar phenolic structure, demonstrated a high removal of 93 ± 3%. Due to the inherent instability of E1, the filtration experiment was repeated, yielding consistent results (92 ± 3% removal).

In contrast to E1 and E2, P is characterized by its ketone group and cyclopentane ring, which contribute to its relatively lower reactivity toward direct electron transfer oxidation. The ketone group, due to its polar carbonyl group, is more prone to engage in nucleophilic addition as an electron acceptor, aligning it more with reduction than oxidation processes.[78,79] Additionally, the cyclopentane ring, as a saturated hydrocarbon, is less reactive than its unsaturated counterparts, further impeding the degradability of P. The proposed pathway for oxidation of P is shown in Equation (2).

Precise structural analysis of specific degraded products using advanced techniques, such as high-resolution LC-MS, is important to identify the precise reaction pathways. Developing suitable analytical methods is currently not possible, especially given the extremely low concentrations involved and the challenges in SH analysis. This area requires further investigation and falls beyond the scope of the current study.

2.5. Electrochemical Degradation of Different Types of Hormones

Given that the degradation of SH is dependent on the chemical structure, the degradability of SH using the CNT EMR was evaluated using different SH estrone (E1), estradiol (E2), testosterone (T), and progesterone (P) (**Figure 5**).

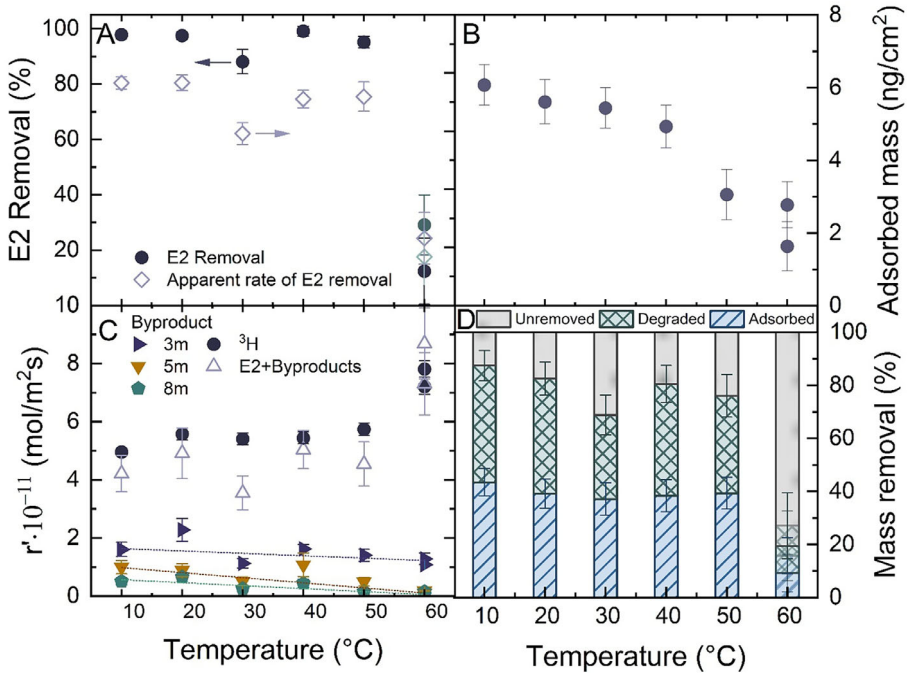

Figure 6. Electrochemical degradation of estradiol (E2) over temperature from 10 to 60 °C, expressed as A) E2 removal and apparent rate of E2 removal, and B) apparent rate of byproduct formation, ^{3}H, and the sum of E2 and the three byproducts; C) adsorbed E2 mass prior to turning the power; and D) contribution to the mass removal of E2 by the electrochemical adsorption and degradation versus temperature. $c_{f,E2}$ = 100 ng L^{-1}, V_{cell} = 1.6 V, J_f = 600 L m^{-2} h^{-1} (2 mL min^{-1}), 1 mM $NaHCO_3$, 10 mM NaCl, 27.2 mg L^{-1} EtOH, 79.2 mg L^{-1} MeOH, pH 8.2 ± 0.2. Error bars represent propagated error from operational parameter variations and analytical error.

2.6. Role of Adsorption in Estradiol Degradation

In the context of surface electron transfer as a heterogeneous process, adsorption of the reactants at the electrode surface serves as a fundamental prerequisite.[80] As discussed in previous sections, the electron transfer rate at the CNT surface is rapid, which means that adsorption and mass transfer processes are potential limiting factors. To ascertain the extent to which adsorption kinetics influence the CNT EMR, a series of temperature-dependent experiments (range of permeate temperatures from 10 to 60 °C) was conducted (**Figure 6**). The concurrent contributions of adsorption and degradation to E2 removal during filtration experiments were distinguished using a previously developed analytical approach that combines UHPLC-FSA and LSC techniques.[61]

The removal of E2 by the CNT membrane remained relatively high, between 90–98%, across a temperature range of 10 to 50 °C (Figure 6A). However, it decreased sharply to 13 ± 12% at 60 °C (Figure 6A). To verify this significant drop, a further experiment was conducted at 60 °C, yielding a similar E2 removal of 29 ± 11%. According to the Arrhenius equation[81] and transition state theory,[82] the electron transfer rate constant typically increases with rising temperature. The observed discontinuity from 50 to 60 °C suggested a range of reaction conditions where the E2 degradation is constrained by the adsorption. The adsorption of E2 onto CNT is likely an exothermic process, releasing energy through interactions like van der Waals forces or π–π interactions.[83] Therefore, low temperatures are expected to favor E2 adsorption on CNT surfaces. This is supported by data of the adsorbed E2 mass on the membrane over the adsorption phase (prior to applying the voltage at 200 mL permeate, Figure 6B). The adsorbed mass of E2 remained nearly constant between 6.1 ± 0.6 and 4.9 ± 0.6 ng cm^{-2} with an increase in temperature from 10 to 40 °C, followed by a rapid drop to 2.7 ± 0.6 ng cm^{-2} when the temperature is further increased to 60 °C. Therefore, the rapid decline in the overall E2 removal rate at 60 °C could be attributed to a reduced adsorption (or increased desorption), which in turn reduced the probability of direct contact between E2 molecules and the electron transfer sites on the CNT surface.

During the electrochemical degradation of E2, the formation rate of byproduct-3m was observed to be relatively stable, varying between (0.9 ± 0.09) × 10^{-11} and (2.2 ± 0.3) × 10^{-11} mol m^{-2} s^{-1} across the 10 to 60 °C temperature range (Figure 6C). In contrast, the formation rates of byproducts-5m and -8m exhibited a decreasing trend with increasing temperature, dropping from (10 ± 0.5) × 10^{-12} to (0.9 ± 0.03) × 10^{-12} mol m^{-2} s^{-1} for byproduct-5m, and from (6.6 ± 1.5) × 10^{-12} to (0.5 ± 0.1) × 10^{-12} mol m^{-2} s^{-1} for byproduct-8m. This pattern suggested that the formation of byproducts-5m and -8m is impeded by the adsorption kinetics of their precursor molecules. These observations align with the prior hypothesis that byproduct-8m or -5m are likely the initial ketone derivatives resulting from the early phase of E2 oxdiation. At elevated temperatures, the formation rate of byproduct-8m and -5m decreased due to a reduction in the adsorption of its precursor, E2.

Among the removed E2 mass from the initial feed, the contributions of adsorption and degradation remained relatively

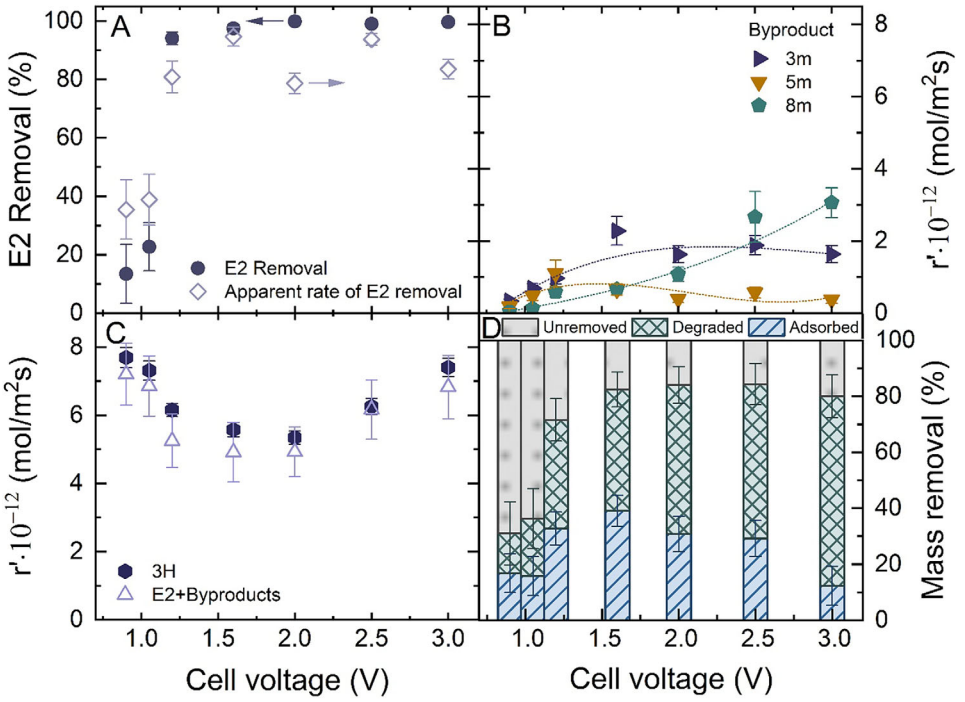

Figure 7. Electrochemical degradation of estradiol (E2) over cell voltage from 0.9 to 3 V, expressed as A) E2 removal and apparent rate of E2 removal, and B) apparent rate of byproduct formation, C) ^{3}H, and the sum of E2 and the three byproducts in permeate; and D) contribution to the mass removal of E2 by the electrochemical adsorption and degradation versus cell voltage. $c_{f,E2}$ = 100 ng L^{-1}, J_f = 600 L m^{-2} h^{-1} (2 mL min^{-1}), 1 mM $NaHCO_3$, 10 mM NaCl, 27.2 mg L^{-1} EtOH, 79.2 mg L^{-1} MeOH, pH 8.2 ± 0.2, 23 ± 0.2 °C. Error bars represent propagated error from operational parameter variations and analytical error.

consistent below 60 °C, whereas both of the degradation and adsorption contributions decreased dramatically at 60 °C (Figure 6D). This aligned with the hypothesis that high temperature impeded the adsorption of E2, thereby hindering the subsequent electrochemical reactions.

2.7. Role of the Electron Transfer in Estradiol Degradation

Upon adsorption onto the membrane surface, the application of a sufficiently high electrochemical potential initiates electron transfer, thereby degrading the micropollutants. The electrochemical filtration experiments, conducted at varying cell voltages ranging from 0.9 to 3 V (0.8–1.8 V vs Ag/AgCl, Figure S4, Supporting Information), were carried out to determine the extent to which the electron transfer rate limits the electrochemical degradation of E2 (**Figure 7**).

When cell voltages of 0.9 and 1.1 V (0.8 and 0.9 V vs Ag/AgCl) were applied, the CNT EMR exhibited relatively low E2 removal of 13 ± 10% and 22 ± 8%, respectively (Figure 7A). Notably, a marginal increase in the cell voltage to 1.2 V (1 V vs Ag/AgCl), which exceeded the necessary potential for E2 electrooxidation, resulted in a substantial enhancement in E2 removal, reaching 94 ± 2%. At voltages above 1.2 V the E2 removal achieved higher than 98%, with concentrations below the LOD. The apparent removal rate reached a plateau at ≈5 ± 0.3 mol m^{-2} s^{-1}. This plateau suggested a surface concentration-limited regime was attained.

As discussed earlier, byproduct-8m or byproduct-5m was postulated to be the initial ketone derivative formed during the early stages of E2 degradation. The results at varying voltages (Figure 7B) suggested that byproduct-5m was more likely to correspond to this initial degraded product. Below 1.2 V, the formation rate of byproduct-5m increased consistently with rising voltage. When voltages increased further, the concentration of byproduct-5m began to decline. This was likely due to further transformation into smaller molecular entities, leading to the increased formation of other byproducts. In contrast, the formation rate of byproduct-8m continued to rise across the entire voltage range, implying that this may be an intermediate formed during the final stages that is resistant to further degradation. Byproducts-3m showed enhanced formation with increasing voltages up to 1.6 V (1.36 V vs Ag/AgCl). Beyond this threshold, its formation rate stabilized, suggesting that the formation of byproduct-3m appears to be predominantly dictated by electron transfer kinetics at voltage <1.6 V, transitioning to a regime controlled by the avaibility of its parent compound above 1.6 V. Increasing the voltage to 3 V did not lead to the formation of "invisible" byproducts in UHPLC chromatography. This was evident because the ^{3}H concentration in the permeate was equivalent to the sum of E2 and detectable byproducts (Figure 7C). This finding confirmed the challenges in degrading byproduct-8m and -3m, which ultimately restricted the complete elimination of E2. While increasing the voltage could potentially facilitate the mineralization of E2 into CO_2 and H_2O, the stability of the CNT electrode at higher voltages will be compromised.

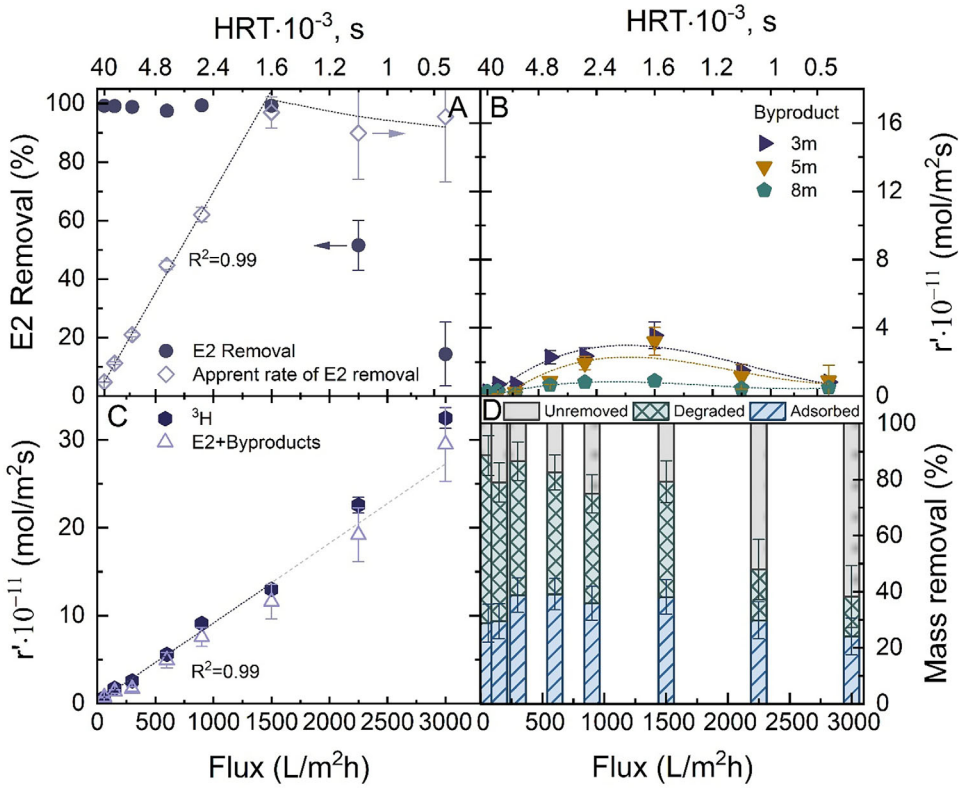

Figure 8. Electrochemical degradation of estradiol (E2) over flux from 60 to 3000 L m^{-2} h^{-1}, expressed as A) E2 removal and apparent rate of E2 removal, and B) apparent rate of byproduct formation, C) ^{3}H, and the sum of E2 and the three byproducts in permeate; and D) contribution to the mass removal of E2 by the electrochemical adsorption and degradation versus flux and hydraulic residence time (HRT). $c_{f,E2}$ = 100 ng L^{-1}, V_{cell} = 1.6 V, 1 mM $NaHCO_3$, 10 mM NaCl, 27.2 mg L^{-1} EtOH, 79.2 mg L^{-1} MeOH, pH 8.2 ± 0.2, 23 ± 0.2 °C. Error bars represent propagated error from operational parameter variations and analytical error.

In addition to being converted into byproducts, some E2 remained adsorbed on the membrane throughout the filtration process. At lower cell voltages (<1.2 V), ≈16 ± 7% of the radiolabeled compounds were quantified as adsorbed on the membrane (Figure 7D). Interestingly, this adsorbed fraction increased, reaching 39 ± 6% when the voltage was raised to 1.6 V. E2 is neutral at pH below the pKa of 10.3 and the local pH near the anode is acidic. The enhanced adsorption can be speculated to originate from a more positive voltage inducing stronger polarization or dipole–dipole interactions between its polar functional groups (—OH) and the electrode surface. As the voltage increased further, more of the adsorbed E2 was transformed into byproducts and subsequently desorbed from the membrane, resulting in a decrease in the adsorption fraction to 12 ± 7% at 3 V. As a result, he contribution of degradation to the overall removal of E2 consistently increased from 14 ± 11% to 68 ± 8%.

2.8. Role of Hydraulic Residence Time in Electrochemical Degradation

In addition to the adsorption and electron transfer rate, the hydraulic residence time (HRT) of micropollutants within the EMR played an important role in determining the interaction dynamics between micropollutants and the membrane. HRT is determined by permeate flowrate or flux, while a higher HRT reduces the pollutant load per unit of time (molar flux). This will increase the probability of a micropollutant molecule to encounter a reactive species and/or adsorb onto the electron transfer sites on the membrane surface. To determine the threshold of HRT for limiting the removal performance of the CNT EMR, a series of experiments at varying water flux from 60 to 3000 L m^{-2} h^{-1} were conducted (**Figure 8**). This corresponds to HRTs of 40 × 10^{-3} to 0.8 × 10^{-3} s, while the molar flux increased from 6.1 × 10^{-12} to 3.1 × 10^{-10} mol m^{-2} s^{-1}. This HRT range is one to two orders of magnitude shorter than that reported for photocatalytic membranes.[27] The reason is the thinner active layer of the CNT membrane compared to the microfiltration membrane with photocatalysts inside the pores. While the greater thickness of photocatalytic membranes can hinder degradation due to inadequate light penetration, this limitation is avoided in electrochemical membranes, where the applied electrochemical potential is uniformly distributed across the CNT coating that offers a very large membrane surface.

A strong linear correlation (R^2 = 0.99) was observed between the HRT and the rate of E2 removal, which increased from (0.8 ± 0.02) × 10^{11} to (17 ± 0.9) × 10^{11} mol m^{-2} s^{-1} when the HRT increased from 1.6 × 10^{-3} to 39.6 × 10^{-3} s. The molar flux decreased from 1.5 × 10^{-10} to 6.1 × 10^{-12} when flux decreased from 1500 to 60 to L m^{-2} h^{-1} (Figure 8A). This implied that

the electrochemical reaction kinetics were limited by the available amount of E2 molecular within the EMR per unit time at the HRT $<1.6 \times 10^{-3}$ s. The rate of E2 removal plateaued with further increases of the flux to 3000 L m^{-2} h^{-1}, transitioning to an electron-transfer limited regime. In this regime, the electrochemical reaction rate is too slow to degrade the high mass of E2 that arrives at the membrane. The sharp transition from mass-limited to electron-transfer-limited regimes could be attributed to the strong dependence of the direct electron transfer mechanism on the availability of electrochemical sites.

The ^{3}H activity in the permeate increased linearly ($R^2 = 0.99$) with flux between 60 and 1500 L m^{-2} h^{-1}, consistent with E2 removal trends, confirming that adsorption was limited by E2 availability. Beyond 1500 L m^{-2} h^{-1}, the deviation from linearity and elevated ^{3}H activity in permeate signified insufficient contact time for adsorption, resulting in untrapped E2 bypassing the membrane. This reduced contact time caused a sharp decline in degradation's contribution (from 41 ± 7 to 14 ± 11%) and adsorption's contribution (from 38 ± 6% to 24 ± 7%) to total removal, as flux rose from 1500 to 3000 L m^{-2} h^{-1} (Figure 8D). These results highlight that, under the given conditions (1.6 V and 100 ng L^{-1}), the influence of contact time on the electrochemical reactions was more pronounced than on adsorption kinetics. This resulted in a shift toward greater mass removal through adsorption rather than degradation, which was supported by the marked reduction in byproduct formation rates at fluxes exceeding 1500 L m^{-2} h^{-1} (Figure 8B).

3. Conclusion

Investigating the complex mechanisms of SH removal via membrane electrocatalysis at environmentally relevant concentrations (50–10^6 ng L^{-1}) is challenging due to the need for suitable analytical tools and a filtration system that captures adsorption/desorption, heterogeneous electron transfer, and indirect degradation processes. This study addresses these challenges by using an ultrafiltration membrane coated with CNTs in a single-pass flow-through EMR system to explore these removal mechanisms and limiting factors. Through an analytical approach combining UHPLC-FSA and LSC, both of which can quantify SH at ng L^{-1} levels, the concurrent electrochemical adsorption and degradation processes within the EMR could be differentiated.

The overestimation of removal performance often reported at high initial concentrations in electrooxidation processes was not observed in the CNT EMR. Instead, the E2 removal rate achieved at high concentrations could be extended to lower concentrations across the feed range of 50 to 5×10^4 ng L^{-1}. This consistency is likely due to the elimination of mass transfer limitations within the EMR, achieved by convective flow and the high surface area of the CNTs that adsorb and preconcentrate micropollutants. Beyond 5×10^4 ng L^{-1}, the system transitions from an E2-availability-limited regime to one constrained by the surface area of the membrane.

The heterogeneous electron transfer predominated the degradation mechanism at the CNT surface. With this, the chemical structure of the micropollutant is the most important factor, determining their electrochemical degradability. A high removal (>90%) could be achieved for E1 and E2 that contain a phenolic group. However, T and P, characterized by a ketone group, exhibited much lower electro-oxidative activity.

For electrochemically degradable compounds like E2, adsorption by the CNT surface was then required before electron transfer could occur. Elevating the temperature from 10 to 60 °C, which reduced the extent of adsorption, resulted in a marked decline in E2 removal abruptly after 50 °C from 97 ± 2% to 13 ± 12%. Upon adsorption of the SH micropollutants on the CNT surface, direct electron transfer occurred if the surface potential exceeded the minimal required threshold of 0.75 V. Thus, increasing the cell voltage from 0.90 to 1.20 V (corresponding to a surface potential increase from 0.76 to 1 V) led to a significant enhancement in E2 removal from 13 ± 10% to 94 ± 2%, where the electron transfer rate limited the degradation rate. Thanks to the combined analytical tools, the contributions of adsorption and degradation to the total mass removed from the initial feed were quantified and found to increase concurrently as the voltage was raised to 1.2 V, despite the neutrality of E2 within the acidic local pH environment near the anode. This increase could be possibly due to stronger polarization or dipole–dipole interactions induced at higher voltages. Beyond 1.2 V, the total removed E2 mass did not significantly increase, as it had nearly reached 100%, with degradation contributing more substantially than adsorption to the removal.

Besides the electron transfer rate, the contact time was another important factor limiting the micropollutant removal. The removal efficiency of E2 was impeded when the HRT was less than 1.6×10^{-3} s, implying that the electrochemical reaction kinetics were restricted by the interaction time between E2 molecules and the CNT interfaces.

These findings offer significant implications for micropollutant control and suggest that the CNT EMR can have significant advantages compared with such emerging technologies as membrane photocatalysis, which are limited by uniform light penetration and the oxidizing capacity of indirect reactive species. Achieving further insights into the reaction mechanisms and limiting factors will be highly beneficial in designing EMR processes for sustainable environmental remediation.

While E2 levels in the permeate after CNT EMR treatment were negligible, high yields of its degradation products were found. Further investigation is needed to verify these results in real water matrices, where the potential increase in toxicity from byproducts poses a significant concern, particularly in the context of estrogenic activity in practical water reuse applications. Additionally, long-term membrane stability and fouling control remain critical for real-world applications. Future work will integrate real-time fouling monitoring and validate stability under extended operational cycles (e.g., >10 000 h).

4. Experimental Section

Electrochemical Filtration System and Protocol: Electrochemical filtration experiments were conducted using a custom-built flow-through EMR system (**Figure 9**A), which is a downscaled adaptation (a 2 cm^2 membrane surface area) of a previously developed larger-scale model[61] that originally featured an effective membrane area of 20 cm^2. A physical image of the system can be found in Figure S1 (Supporting Information). A comprehensive hydrodynamic analysis of this system is available elsewhere.[84] This miniaturization was designed to facilitate an in-depth investigation of

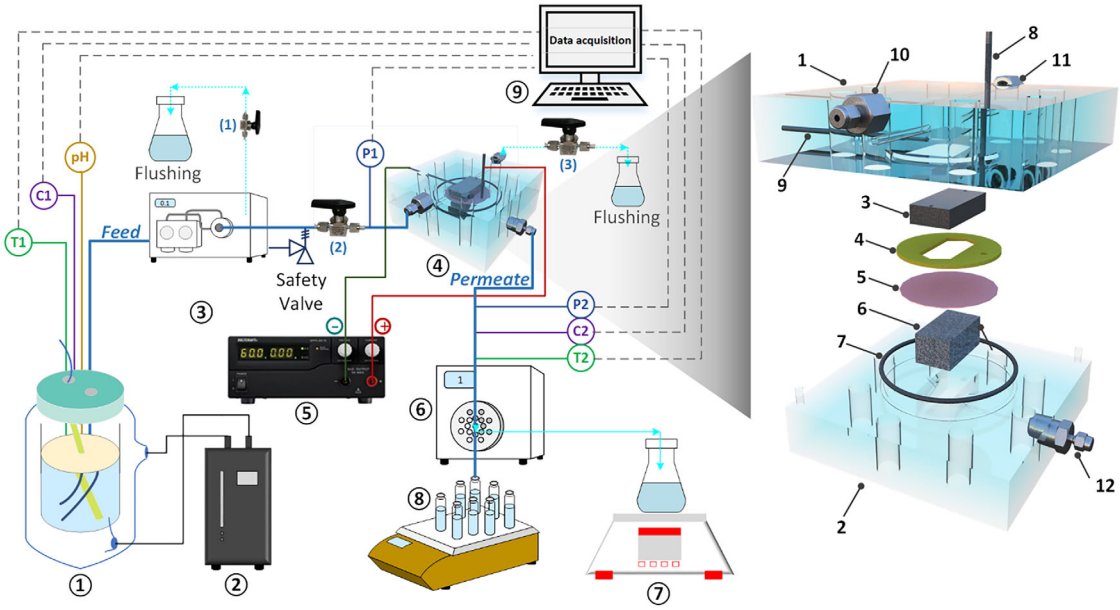

Figure 9. (Left) Schematic diagram of the flow-through electrochemical membrane reactor system, ① double-wall jacketed feel bottle (1 L), ② chiller, ③ double piston pump, ④ electrochemical membrane cell, ⑤ electric power supply, ⑥ 16-port switching valve, ⑦ balance, ⑧ sample vials, and ⑨ data acquisition card (DAQ). (Right) Schematic diagram of the exploded view, and side view of the electrochemical membrane reactor, 1 top cell, 2 bottom cell, 3 titanium cathode, 4 PEEK spacer, 5 electrochemical membrane, 6 titanium porous support, 7 O-ring, 8 platinum wire, 9 titanium wire, 10 feed inlet connector, 11 crossflow outlet connector, and 12 permeate outlet connector.

the mechanisms and various limiting factors that arise at environmentally relevant concentrations.

The core element of the filtration system is an electrochemical filtration cell ④ that was designed in-house and manufactured by Shenzhen Rapid Direct Co., Ltd., (China). The cell was constructed using acrylic material, with a titanium sheet (thickness 3.5 mm, Kunshan Shangte New Materials Technology Co., Ltd., China) being embedded as the counter electrode (Figure 9B). Elaborated specifics regarding the reactor configuration are given in Supporting Information. Details of other key components can also be found in Supporting Information. The experimental protocol (Table S1, Supporting Information) was adapted from a previous methodology designed for a similar photocatalytic filtration setup,[26] with the modification of substituting the LED light source with the electrical power source.

Solution chemistry and operating parameters throughout the filtration process, including conductivity, temperature, pH, and transmembrane pressure were monitored using sensors in all experiments using applicable sensors. The acquired data were collected via the DAQ card. Comprehensive information for the details is given in the Supporting Information.

Electrochemical Membrane Preparation and Characterization: A poly(ether sulfone) (PES) ultrafiltration (UF) membrane coated with a CNT layer was used. The preparation of the CNT membrane followed the methodology developed by Zhu et al.[85] Details regarding the preparation process are shown in the Supporting Information.

The surface morphology of the CNT membrane was examined using scanning electron microscopy (SEM, FEI XL30 SEM-FEG, Hillsboro, USA). Based on the SEM images, the thickness of the formed CNT layer was ≈2 µm and the pore diameter ≈0.125 µm.[86] The surface resistivity of the CNT membrane was estimated to be 0.072 Ω cm using a Four-point probe (4PP) source meter (2611A, KEITHLEY, USA) with a probe head (Signatone, USA),[87] as described in previous work.[61] The surfaces of the CNT membranes were found to be negatively charged across a pH range of 2–10 in an electrolyte containing 10 mM NaCl, as determined using a SurPASS Analyzer (Anton Paar GmbH, Graz, Austria).[61] The membrane permeability was determined to be 317 ± 7 L m^{-2} h^{-1} × bar with MilliQ water (Figure S2, Supporting Information).

The surface potential of the membrane versus an Ag/AgCl reference was measured at various cell voltages ex situ using the open circuit potential method.[88] These measurements utilized a potentiostat (Zennium Pro, Zahner, Germany) in a three-electrode setup (Plate Material Evaluating Cell, Teflon, ALS, Japan) with an electrolyte containing 10 mM NaCl and 1 mM $NaHCO_3$. Figure S3 (Supporting Information) illustrates the setup configuration. The surface potential of the CNT membrane versus the Ag/AgCl reference was determined to be 1.3 V (Figure S4, Supporting Information) at a standard cell voltage of 1.6 V.

The electrochemical stability of the CNT membrane as an anode was assessed using an electrode polarization curve, which showed the current passing through the system over time at a fixed anodic potential. This curve was measured with a potentiostat in a three-electrode setup. The results (Figure S5, Supporting Information) indicated that the CNT membrane remained stable at a potential of 1.2 V within 24 h of measurement. However, signs of CNT decomposition were observed at 1.5 V (equivalent to a cell voltage of 2 V, Figure S4, Supporting Information).

Steroid Hormone and Solution Chemistry: Four radiolabeled SHs were utilized in this study: [2,4,6,7-^{3}H] estrone (E1); [2,4,6,7-^{3}H]-estradiol (E2), [1,2,6,7-^{3}H] progesterone (P), [1,2,6,7-^{3}H] testosterone (T). Radiolabeled E2, P, and T were provided in pure ethanol (EtOH) solution by PerkinElmer LAS GmbH (Germany) and stored at −20 °C. E1 was supplied by Biotrend Chemikalien GmbH (Germany) under the same storage conditions. The hydrodynamic (Stokes) diameter of SH was ≈0.8 nm,[89] which was significantly smaller than the pore diameters of both the CNT layers (125 nm) and the PES support (3.8 nm). Due to this substantial size disparity, SH could not be retained by the membrane through size exclusion. Other essential characteristics of the SHs are summarized in Table S2 (Supporting Information).

The methodology of preparing the SH feed solution with varying concentrations in a background electrolyte is provided in the Supporting Information. Given the limited solubility of SHs in aqueous media, additional MeOH was introduced into the feed solutions, resulting in a consistent concentration of 79.2 mg L^{-1} MeOH and 26.3 mg L^{-1} EtOH within all the feed solutions. The high concentrations of MeOH and EtOH may modify the degradation mechanism within the EMR by scavenging •OH

with a high reaction rate ($k_{MeOH,\cdot OH} = 9.7 \times 10^8 M^{-1}s^{-1}$, and $k_{EtOH,\cdot OH} = (1.2 - 2.8) \times 10^9 M^{-1}\ s^{-1}$[90]). Owing to the inherent characteristics of the radiolabeled SH experiment, conducting experiments devoid of solvent presence was unattainable. To at least work on the same solvent concentration, the ultimate concentrations of EtOH and MeOH within all feed solutions remained fixed at 26.3 and 79.2 mg L^{-1}, respectively.

To examine whether E2 evaporates with high vapor pressure solvents (12.8 kPa for both MeOH and EtOH (88)), changes in E2 and TOC concentrations (measured with a TOC-L CPH, Shimadzu, Japan) in the feed solution were tracked over 19 h of freeze drying (Alpha 2–4 LSCplus, Martin Christ, Germany). Results (Figure S6, Supporting Information) show that both E2 concentration and TOC levels decreased as a function of freeze drying time, suggesting that E2 might be evaporating along with the solvent. To prevent E2 loss during filtration, the feed tank had to be covered, with three feed samples collected to verify the concentration at the beginning, midway through, and at the end of filtration.

Analytical Methods for Water Quality: The separation and quantification of intact SHs were performed using a modified variant of the ultra-high-performance liquid chromatography (UHPLC, Flexar, Perkin Elmer, USA) method, integrated with a flow scintillation analyzer (FSA, Radiomatic 625TR, Perkin Elmer, USA). This UHPLC-FSA method, developed by Lyubimenko et al.[91] had been adapted by altering the elution time (reduced from 25 to 15 min), injection volume (increased from 100 to 200 µL), and mobile phase flow rate (changed from 0.25 to 0.2 mL min^{-1}), achieving a limit of detection (LOD) as low as 2.5 ng L^{-1} for E2 (Figure S7, Supporting Information). An overview of the current elution parameters and details of the analytical procedure can be found in Table S3 (Supporting Information).

The quantification of overall ^3H activity in the sample, including the radiolabeled SHs and their degraded products, was carried out with a liquid scintillation counter (LSC, 2550 TR/AB, Packard, USA) method.[92] Sample preparation for LSC analysis involved mixing 1 mL of the sample with 1 mL of scintillation cocktail (Ultima Gold LLT, Perkin Elmer, USA). The measurement was performed in triplicate, and the duration of each measurement was 10 min, achieving a LOD of 0.1 ng L^{-1}.

The combination of UHPLC-FSA and LSC analysis enabled differentiation of the complex concurrent degradation and adsorption processes during SH removal, thereby providing a deeper understanding of the underlying mechanisms within the EMR for micropollutant removal.

Electrochemistry of Steroid Hormones: Cyclic voltammetry (CV) measurements were conducted using a Zennium Pro potentiostat (Zahner, Germany) to analyze the electrochemistry of SH micropollutants on the CNT membrane. These measurements were performed over a potential range from 0 to 0.9 V at a scan rate of 100 mV s^{-1}, utilizing a three-electrode cell (Plate Material Evaluating Cell, Teflon, ALS, Japan, Figure S3, Supporting Information). In this setup, the CNT membrane served as the working electrode, a Pt wire (Φ0.5 mm, ALS, Japan) functioned as the counter electrode, and an Ag/AgCl electrode (Redox.me, Sweden) was used as the reference electrode.

Prior to the CV measurement, the membrane was pre-filtered with 20 mL of 1 mg L^{-1} SH solution prepared in the electrolyte consisted of 1 mM $NaCO_3$, 10 mM NaCl to enhance the adsorption. Subsequently, the measurement was conducted in a fresh SH solution, maintaining the same compositional constituents.

Identification and Quantification of Reactive Species: The primary reactive species, responsible for the removal of E2 in the EMR process, were identified by scavenging experiments, which rely on the principle of disparities in reaction rates between potential reactive species and scavengers.[93,94] Sodium nitrate ($NaNO_3$, >99.5% purity, Merck, Germany) was chosen as the scavenger to ascertain the contributions of surface electrons (e^-) based on the published rate constant ($k_{NO_3^-,e^-} = 9.7 \times 10^9$[90]). In the scavenging experiments, the filtration was carried out under standard conditions with added 10 mM $NaNO_3$ into the feed solution.

Another potential reactive species, •OH,[95] was quantitatively analyzed under varying conditions using the chemical probe, coumarin. A feed solution containing 0.01 mM coumarin was subjected to filtration in the CNT EMR with the electric power activated. The byproduct, 7-hydroxycoumarin, resulting from the hydroxylation reaction between coumarin and ·OH, was measured using a fluorescence spectrophotometer (Cary, Eclipse Varian, Agilent, US) at an excitation wavelength (λ_{ex}) of 330 nm.[96]

When Cl^- was present in the feed solution as dissolved state, active chlorine (Cl_2, Cl·, HClO, and ClO^-) was electrochemically produced by oxidation of the dissolved Cl^- at the anode surface, as described via reactions Equations (S1)–(S5, Supporting Information).[97] The production of active chlorine in the EMR at varying voltage was quantitatively compared using the Wessler reaction, which involved the oxidation of iodide ions (I^-) into iodine (I_2),[98] as detailed in Supporting Information. This method was validated using electrochemically generated active chlorine, achieved through two platinum wire electrodes (50HX15 0.6/250MM, Redox.me, Sweden) in a 10 mM of NaCl electrolyte (Figure S8, Supporting Information).

Data Processing and Error Propagation: Membrane performance equations in terms of the pure water flux (J_w, L m^{-2} h^{-1}), permeability (L, L m^{-2} h^{-1} × bar), and mean HRT (s) are given in Table S4 (Supporting Information).

The removal of SH (R, %) was utilized to evaluate the SH removal efficiency at steady-state conditions, which was defined via Equation (3).

$$R = \left(1 - \frac{c_{p,eq}}{c_f}\right) \times 100 \tag{3}$$

where c_f (ng L^{-1}) is the feed SH concentration; $c_{p,\,eq}$ (ng L^{-1}) is the SH concentration of the permeate at steady-state, determined at the end of the experiment (cumulative permeate volume V_p = 700 mL). To rectify inaccuracies arising from fluctuations in data points when determining the R, $c_{p,\,eq}/c_f$ value was ascertained through the fitting of experimental data $c_{p,\,eq}/c_f$ versus V_p to an exponential model, which is elucidated in detail in Figure S10 (Supporting Information).[27]

The assessment of SH degradation kinetics using the CNTs EMR was assessed upon the determination of the apparent rate of SH removal (r'_{SH}, mol m^{-2} s^{-1}), as described in previous work.[26] This parameter quantifies the cumulative amount of SH removed per membrane unit area, per unit of time, over the 700 mL filtration experiment.

$$r'_{rem} = \frac{m_{rem}}{t \times M \times A} = \frac{m_{rem} \times J_{SH}}{3600 \times M \times V} \tag{4}$$

where t (s) is the time duration of the filtration experiments, M (ng mol^{-1}) is the molecular weight (MW) of the studied SH, A (2×10^{-4} m^2) is the effective membrane surface area, J_{SH} (L m^{-2} h^{-1}) is the flux of SH solution, V (0.7 L) is the total filtration volume, m_{rem} (ng) is the total mass of SH removed over the 700 mL of filtration experiment, including both the adsorption and degradation phases. The quantification of m_{SH} involved the curve fitting and integration of the experimental data of SH concentration in permeate ($c_{p,SH}$, ng L^{-1}) across the range of permeate volume, which is explained in Figure S11 (Supporting Information).

To evaluate the kinetics of generating a specific byproduct throughout the electrochemical degradation process, the parameter apparent rate of byproduct formation (r'_{prod}, mol m^{-2} s^{-1}) was quantified using Equation (5).

$$r'_{prod} = \frac{m_{prod}}{t_{deg} \times M \times A} = \frac{m_{prod} \times J_{SH}}{3600 \times M \times V_{deg,SH}} \tag{5}$$

where t_{deg} (s) is the time duration of the electrochemical degradation phase (500 mL), $V_{deg,SH}$ (0.5 L) is the accumulative volume encompassing the degradation phase, m_{prod} (ng) represents the cumulative mass of the specific byproduct in the permeate within the electrochemical degradation process. Figure S12 (Supporting Information) exemplifies the determination of the m_{prod} by fitting and integrating the data points of the byproduct concentration in the permeate ($c_{p,prod}$, ng L^{-1}) over the permeate volume. Since the radiolabeled byproducts of SH were not commercially available, the calibration curve for SH was used for the quantification

of its byproducts. Note that the concentrations determined using the SH calibration did not reflect the actual levels of each byproduct. Instead, they were employed to enable quantitative comparisons of the formation of each byproduct under varying conditions. For example, the ketone derivative, as a potential byproduct of E2 that contained four ^{3}H atoms, would yield the same peak area as E2. However, its concentration in ng L^{-1} would be lower due to the loss of two protons.

The contribution of electrochemical adsorption (θ_{ads}, %) and degradation (θ_{deg}, %) within the EMR to the total mass of SH in feed can be estimated via Equations (6) and (7).

$$\theta_{ads} = \frac{m_{ads}}{m_f} \tag{6}$$

$$\theta_{deg} = \frac{m_{deg}}{m_{rem}} = \frac{m_{rem} - m_{ads}}{m_f} \tag{7}$$

where m_{ads} (ng) is the total mass of the SH and its byproducts adsorbed on the membrane, which is derived from the data of ^{3}H activity in the permeate (Figure S13, Supporting Information). Due to the inability to identify the electrochemical byproducts of SH, the concentration of the mixture containing both SH and its byproducts in the permeate is determined using the calibration curve of LSC for SH. m_{deg} (g) is the total mass of the SH removed by degradation over the experiment, which could be determined by the difference between the mass of total removed SH (m_{rem}, g) and adsorbed SH (m_{ads}, g).

The estimation of errors in SH concentration was performed using the error propagation method,[99,100] which considered variations from multiple sources including solution preparation, the filtration system, and analytical devices. Details on these specific sources and their estimated relative errors are provided in Table S5 (Supporting Information). The reproducibility of E2 electrochemical degradation was assessed through five experimental repetitions under standard conditions (Figure S15, Supporting Information). The results showed an E2 removal rate of 97 ± 1%, aligning closely with the error margin estimated through error propagation methods.

Supporting Information

Supporting Information is available from the Wiley Online Library or from the author.

Acknowledgements

The authors express their gratitude to Helmholtz Recruitment Initiative for funding of IAMT (A.I.S); and Bundesministerium für Bildung und Forschung (BMBF) project, NanoElectroMembrane processes for micropollutant removal in water reuse (NEMWARE), (A.I.S), Special thanks go to Mr. Mohammed Basith Abdul Khader Basheer Ahamed (KIT-IAMT) for his diligent experimental work of the electrochemical filtrations; Dr. Xiaobo Zhu for fabricating the CNT electrochemical membranes.

Open access funding enabled and organized by Projekt DEAL.

Conflict of Interest

The authors declare no conflict of interest.

Author Contributions

Conceptualization was done by S.L. and A.I.S. Methodology was done by S.L., D.J., and A.I.S. Validation was done by S.L. Formal analysis was done by S.L. Original draft was written by S.L. S.L., D.J., and A.I.S. dealt with writing the review and editing. Supervision was done by A.I.S. Project administration was done by A.I.S. Funding acquisition was done by A.I.S.

Data Availability Statement

The data that support the findings of this study are available from the corresponding author upon reasonable request.

Keywords

by-product transformation, electrochemical membranes, heterogeneous electron transfer, physio-chemical water treatment, single-pass ultrafiltration

Received: April 29, 2025
Revised: July 25, 2025
Published online:

[1] B. I. Escher, H. M. Stapleton, E. L. Schymanski, *Science* **2020**, *367*, 388.
[2] R. P. Schwarzenbach, B. I. Escher, K. Fenner, T. B. Hofstetter, C. A. Johnson, U. V. Gunten, B. Wehrli, *Science* **2006**, *313*, 1072.
[3] D. J. Panyard, B. Yu, M. P. Snyder, *Sci. Adv.* **2022**, *8*, add6155.
[4] M. O. Barbosa, N. F. F. Moreira, A. R. Ribeiro, M. F. R. Pereira, A. M. T. Silva, *Water Res.* **2016**, *94*, 257.
[5] L. M. Bexfield, P. L. Toccalino, K. Belitz, W. T. Foreman, E. T. Furlong, *Environ. Sci. Technol.* **2019**, *53*, 2950.
[6] S. Fekadu, E. Alemayehu, R. Dewil, *Sci. Total Environ.* **2019**, *654*, 324.
[7] J. O. Ojoghoro, M. D. Scrimshaw, J. P. Sumpter, *Sci. Total Environ.* **2021**, *792*, 148306.
[8] M. A. La Merrill, L. N. Vandenberg, M. T. Smith, W. Goodson, P. Browne, H. B. Patisaul, K. Z. Guyton, A. Kortenkamp, V. J. Cogliano, T. J. Woodruff, L. Rieswijk, H. Sone, K. S. Korach, A. C. Gore, L. Zeise, R. T. Zoeller, *Nat. Rev. Endocrinol.* **2020**, *16*, 45.
[9] D. Zhang, C. Lee, H. Javed, P. Yu, J.-H. Kim, P. J. J. Alvarez, *Environ. Sci. Technol.* **2018**, *52*, 12402.
[10] M. Čelić, B. D. Škrbić, S. Insa, J. Živančev, M. Gros, M. Petrović, *Environ. Pollut.* **2020**, *262*, 114344.
[11] K. Lei, C.-Y. Lin, Y. Zhu, W. Chen, H.-Y. Pan, Z. Sun, A. Sweetman, Q. Zhang, M.-C. He, *J. Hazard. Mater.* **2020**, *389*, 121891.
[12] B. Yilmaz, H. Terekeci, S. Sandal, F. Kelestimur, *Rev. Endocr. Metab. Disord.* **2020**, *21*, 127.
[13] V. Kumar, A. C. Johnson, A. Trubiroha, J. Tumová, M. Ihara, R. Grabic, W. Kloas, H. Tanaka, H. K. Kroupová, *Environ. Sci. Technol.* **2015**, *49*, 2625.
[14] Water framework directive watch list method analysis of 17β-estradiol and estrone European Commission, https://publications.jrc.ec.europa.eu/repository/bitstream/JRC94947/lb-na-27970-en-n.pdf, Access date: 27/09/2024, **2016**.
[15] Z. H. Liu, Z. Dang, H. Yin, Y. Liu, *Water Res.* **2021**, *188*, 116469.
[16] N. Zwart, W. Jonker, R. Broek, J. de Boer, G. Somsen, J. Kool, T. Hamers, C. J. Houtman, M. H. Lamoree, *Water Res.* **2020**, *168*, 115204.
[17] P. Šauer, A. Stará, O. Golovko, O. Valentová, A. Bořík, R. Grabic, H. K. Kroupová, *Water Res.* **2018**, *137*, 64.
[18] L. D. Nghiem, A. I. Schäfer, M. Elimelech, *Environ. Sci. Technol.* **2004**, *38*, 1888.
[19] Y.-l. Liu, X.-m. Wang, H.-w. Yang, Y. F. Xie, *J. Membr. Sci.* **2018**, *551*, 37.
[20] A. Imbrogno, A. I. Schäfer, *Sep. Purif. Technol.* **2021**, *267*, 118406.
[21] M. A. Shannon, P. W. Bohn, M. Elimelech, J. G. Georgiadis, B. J. Mariñas, A. M. Mayes, *Nature* **2008**, *452*, 301.
[22] L. Giorno, *Nat. Nanotechnol.* **2022**, *17*, 334.
[23] A. Imbrogno, P. Samanta, A. I. Schäfer, *Environ. Chem.* **2019**, *16*, 630.

[24] S. Dekkouche, S. Morales-Torres, A. R. Ribeiro, J. L. Faria, C. Fontàs, O. Kebiche-Senhadji, A. M. T. Silva, *Chem. Eng. J.* **2022**, *427*, 131476.
[25] Y. Qing, Y. Li, Z. Guo, Y. Yang, W. Li, *J. Environ. Chem. Eng.* **2022**, *10*, 108648.
[26] S. Lotfi, K. Fischer, A. Schulze, A. I. Schäfer, *Nat. Nanotechnol.* **2022**, *17*, 417.
[27] S. Liu, E. Véron, S. Lotfi, K. Fischer, A. Schulze, A. I. Schäfer, *J. Hazard. Mater.* **2023**, *447*, 130832.
[28] B. P. Chaplin, *Acc. Chem. Res.* **2019**, *52*, 596.
[29] C. Comninellis, G. Chen, *Electrochemistry for the Environment*, 1st ed., Springer, New York, NY, USA, **2010**.
[30] B. C. Hodges, E. L. Cates, J.-H. Kim, *Nat. Nanotechnol.* **2018**, *13*, 642.
[31] A. J. Bard, L. R. Faulkner, H. S. White, *Electrochemical Methods: Fundamentals and Applications*, John Wiley & Sons, Hoboken, NJ, USA, **2022**.
[32] R. A. Marcus, *J. Chem. Phys.* **1965**, *43*, 679.
[33] M. M. Ngundi, O. A. Sadik, T. Yamaguchi, S.-i. Suye, *Electrochem. Commun.* **2003**, *5*, 61.
[34] M. A. Alkhadra, X. Su, M. E. Suss, H. Tian, E. N. Guyes, A. N. Shocron, K. M. Conforti, J. P. de Souza, N. Kim, M. Tedesco, K. Khoiruddin, I. G. Wenten, J. G. Santiago, T. A. Hatton, M. Z. Bazant, *Chem. Rev.* **2022**, *122*, 13547.
[35] C. Lin, Z. Shan, C. Dong, Y. Lu, W. Meng, G. Zhang, B. Cai, G. Su, J. H. Park, K. Zhang, *Sci. Adv.* **2023**, *9*, adi9442.
[36] T. Liu, S. Xiao, N. Li, J. Chen, X. Zhou, Y. Qian, C.-H. Huang, Y. Zhang, *Nat. Commun.* **2023**, *14*, 2881.
[37] S. Gligorovski, R. Strekowski, S. Barbati, D. Vione, *Chem. Rev.* **2015**, *115*, 13051.
[38] H. Dodgen, H. Taube, *J. Am. Chem. Soc.* **1949**, *71*, 2501.
[39] S. Neodo, D. Rosestolato, S. Ferro, A. De Battisti, *Electrochim. Acta* **2012**, *80*, 282.
[40] R. Wei, S. Pei, Y. Yu, J. Zhang, Y. Liu, S. You, *Environ. Sci. Technol.* **2023**, *57*, 17404.
[41] Y. Kang, Z. Gu, B. Ma, W. Zhang, J. Sun, X. Huang, C. Hu, W. Choi, J. Qu, *Nat. Commun.* **2023**, *14*, 6590.
[42] Y. Chen, G. Zhang, Q. Ji, H. Lan, H. Liu, J. Qu, *Environ. Sci. Technol.* **2022**, *56*, 9722.
[43] Q. Ji, D. Yu, G. Zhang, H. Lan, H. Liu, J. Qu, *Environ. Sci. Technol.* **2015**, *49*, 13534.
[44] G. Gao, C. D. Vecitis, *ACS Appl. Mater.* **2012**, *4*, 6096.
[45] Y. Zhao, M. Sun, L. R. Winter, S. Lin, Z. Wang, J. C. Crittenden, J. Ma, *Environ. Sci. Technol.* **2022**, *56*, 3832.
[46] Y. He, P. Zhang, H. Huang, X. Wang, B. Chen, Z. Guo, H. Lin, *Sep. Purif. Technol.* **2020**, *251*, 117284.
[47] L. Liu, H. Lan, Y. Cui, Q. Tang, J. Bai, X. An, M. Sun, H. Liu, J. Qu, *Sci. Adv.* **2024**, *10*, adn8696.
[48] M. Sun, X. Wang, L. R. Winter, Y. Zhao, W. Ma, T. Hedtke, J.-H. Kim, M. Elimelech, *ACS EST Engg.* **2021**, *1*, 725.
[49] H. Liu, C. D. Vecitis, *J. Phys. Chem. C* **2012**, *116*, 374.
[50] Q. Ji, G. Zhang, H. Liu, R. Liu, J. Qu, *Environ. Sci. Technol.* **2019**, *53*, 2713.
[51] I. A. Kinloch, J. Suhr, J. Lou, R. J. Young, P. M. Ajayan, *Science* **2018**, *362*, 547.
[52] M. F. L. De Volder, S. H. Tawfick, R. H. Baughman, A. J. Hart, *Science* **2013**, *339*, 535.
[53] S. Iijima, *Nature* **1991**, *354*, 56.
[54] T. W. Ebbesen, H. J. Lezec, H. Hiura, J. W. Bennett, H. F. Ghaemi, T. Thio, *Nature* **1996**, *382*, 54.
[55] A. Peigney, C. Laurent, E. Flahaut, R. R. Bacsa, A. Rousset, *Carbon* **2001**, *39*, 507.
[56] F. Tournus, S. Latil, M. I. Heggie, *Phys. Rev. B* **2005**, *72*, 075431.
[57] A. Takakura, K. Beppu, T. Nishihara, A. Fukui, T. Kozeki, T. Namazu, Y. Miyauchi, K. Itami, *Nat. Commun.* **2019**, *10*, 3040.
[58] Y. Liu, H. Liu, Z. Zhou, T. Wang, C. N. Ong, C. D. Vecitis, *Environ. Sci. Technol.* **2015**, *49*, 7974.
[59] Gd. S. Cunha, B. Md. Souza-Chaves, D. M. Bila, J. P. Bassin, C. D. Vecitis, M. Dezotti, *Sci. Total Environ.* **2019**, *678*, 448.
[60] J. Radjenovic, N. Duinslaeger, S. S. Avval, B. P. Chaplin, *Environ. Sci. Technol.* **2020**, *54*, 14815.
[61] S. Liu, D. Jassby, D. Mandler, A. I. Schäfer, *Nat. Commun.* **2024**, *15*, 9524.
[62] K. Jiang, S. Back, A. J. Akey, C. Xia, Y. Hu, W. Liang, D. Schaak, E. Stavitski, J. K. Nørskov, S. Siahrostami, H. Wang, *Nat. Commun.* **2019**, *10*, 3997.
[63] W.-L. Wang, Q.-Y. Wu, N. Huang, T. Wang, H.-Y. Hu, *Water Res.* **2016**, *98*, 190.
[64] E. Brillas, I. Sirés, in: *Environmental Chemistry for a Sustainable World: Remediation of Air and Water Pollution*, (Eds.: E. Lichtfouse, J. Schwarzbauer, D. Robert), Springer, Dordrecht, Netherlands, **2012**, pp. 297–346.
[65] C. Comninellis, *Electrochim. Acta* **1994**, *39*, 1857.
[66] B. Marselli, J. Garcia-Gomez, P. A. Michaud, M. A. Rodrigo, C. Comninellis, *J. Electrochem. Soc.* **2003**, *150*, D79.
[67] S. Liu, P. C. Edara, A. I. Schäfer, *Water Res.* **2023**, *245*, 120438.
[68] C. Sandford, M. A. Edwards, K. J. Klunder, D. P. Hickey, M. Li, K. Barman, M. S. Sigman, H. S. White, S. D. Minteer, *Chem. Sci.* **2019**, *10*, 6404.
[69] C. A. Martínez-Huitle, M. A. Rodrigo, I. Sirés, O. Scialdone, *Chem. Rev.* **2015**, *115*, 13362.
[70] Y. Ohko, K.-i. Iuchi, C. Niwa, T. Tatsuma, T. Nakashima, T. Iguchi, Y. Kubota, A. Fujishima, *Environ. Sci. Technol.* **2002**, *36*, 4175.
[71] J. Mai, W. Sun, L. Xiong, Y. Liu, J. Ni, *Chemosphere* **2008**, *73*, 600.
[72] Y. Zhao, J. Hu, W. Jin, *Environ. Sci. Technol.* **2008**, *42*, 5277.
[73] A. M. Brzozowski, A. C. W. Pike, Z. Dauter, R. E. Hubbard, T. Bonn, O. Engström, L. Öhman, G. L. Greene, J.-Å. Gustafsson, M. Carlquist, *Nature* **1997**, *389*, 753.
[74] M. Arvand, S. Hemmati, *Talanta* **2017**, *174*, 243.
[75] J. Chen, J. Yang, L. Ma, J. Li, N. Shahzad, C. K. Kim, *Sci. Rep.* **2020**, *10*, 2611.
[76] L. Sévery, J. Szczerbiński, M. Taskin, I. Tuncay, F. B. Nunes, C. Cignarella, G. Tocci, O. Blacque, J. Osterwalder, R. Zenobi, M. Iannuzzi, S. D. Tilley, *Nat. Chem.* **2021**, *13*, 523.
[77] J. McMurry, *Organic Chemistry*, Brooks/Cole Thomson Learning, Belmont, CA, **2004**, 497.
[78] A. Burrows, J. Holman, S. Lancaster, A. Parsons, T. Overton, G. Pilling, G. Price, *Introducing Inorganic, Organic and Physical Chemistry*, Oxford University Press, Oxford, England, **2021**.
[79] H. Stetter, H. Kuhlmann, *Org. React.* **2004**, *40*, 407.
[80] S. Saini, J. Halldin Stenlid, F. Abild-Pedersen, *npj Comput. Mater.* **2022**, *8*, 163.
[81] M. R. Bermejo, J. Gómez, A. M. Martínez, E. Barrado, Y. Castrillejo, *Electrochim. Acta* **2008**, *53*, 5106.
[82] H. Eyring, S. Lin, *Basic Chemical Kinetics*, Wiley-Interscience, New York, NY, USA, **1980**.
[83] E. D. V. Duarte, M. G. Oliveira, M. P. Spaolonzi, H. P. S. Costa, T. L. D. Silva, M. G. C. D. Silva, M. G. A. Vieira, *J. Cleaner Prod.* **2022**, *372*, 133743.
[84] A. Imbrogno, A. I. Schäfer, *J. Membr. Sci.* **2019**, *585*, 67.
[85] X. Zhu, A. V. Dudchenko, C. M. Khor, X. He, G. Z. Ramon, D. Jassby, *Environ. Sci. Technol.* **2018**, *52*, 11591.
[86] W. Duan, A. Dudchenko, E. Mende, C. Flyer, X. Zhu, D. Jassby, *Environ. Sci. Process. Impacts* **2014**, *16*, 1300.
[87] L. J. V. D. Pauw, *Philips Res. Rep.* **1958**, *13*, 1.
[88] H. Lee, S. W. Yoon, E. J. Kim, J. Park, *Nano Lett.* **2007**, *7*, 778.
[89] H. L. Bridle, M. B. Heringa, A. I. Schäfer, *Nat. Protoc.* **2016**, *11*, 1328.
[90] G. V. Buxton, C. L. Greenstock, W. P. Helman, A. B. Ross, *J. Phys. Chem. Ref. Data* **1988**, *17*, 513.

[91] R. Lyubimenko, B. S. Richards, A. Turshatov, A. I. Schäfer, *Sci. Rep.* **2020**, *10*, 7095.
[92] J. B. Birks, *Solutes and Solvents for Liquid Scintillation Counting*, Koch-Light Laboratories, London, UK, **1969**.
[93] L. Wang, X. Lan, W. Peng, Z. Wang, *J. Hazard. Mater.* **2021**, *408*, 124436.
[94] J. Wang, S. Wang, *Chem. Eng. J.* **2020**, *401*, 126158.
[95] Y. Yang, *Front. Environ. Sci. Eng.* **2020**, *14*, 85.
[96] Y. Nosaka, A. Y. Nosaka, *Chem. Rev.* **2017**, *117*, 11302.
[97] H. B. Ammar, M. B. Brahim, R. Abdelhédi, Y. Samet, *Sep. Purif. Technol.* **2016**, *157*, 9.
[98] J. D. García-Espinoza, P. Mijaylova-Nacheva, M. Avilés-Flores, *Chemosphere* **2018**, *192*, 142.
[99] J. R. Taylor, W. Thompson, *An Introduction to Error Analysis: The Study of Uncertainties in Physical Measurements*, Springer, New York, NY, USA, **1982**.
[100] A. Imbrogno, M. N. Nguyen, A. I. Schäfer, *Chemosphere* **2024**, *357*, 141833.